ELSEVIER

Materials Science and Engineering A 427 (2006) 27–34

MATERIALS SCIENCE & ENGINEERING A

www.elsevier.com/locate/msea

In situ formation of aluminide intermetallic particles in a magnesium alloy

Hai Zhi Ye, Xing Yang Liu *

Integrated Manufacturing Technologies Institute, National Research Council of Canada, London, Ont., Canada N6G 4X8

Received 14 July 2005; received in revised form 3 March 2006; accepted 20 March 2006

Abstract

Adding nickel to a magnesium alloy (AM60B) during melting produced two types of intermetallic particles in the alloy: manganese nickel aluminide ($Al_{60}Mn_{11}Ni_4$) and nickel aluminide ($Al_{0.42}Ni_{0.58}$). The addition of 0.5 wt.% of Ni by wire dissolution resulted in the formation of $Al_{60}Mn_{11}Ni_4$ particles that were normally fine and uniformly distributed in the cast ingot, promoting grain refinement and significant improvement of tensile properties. $Al_{0.42}Ni_{0.58}$ particles were formed when nickel was added in powder form, and the particles were prone to coarsening and segregation during the melting process.

Keywords: Aluminide particles; In situ formation; Magnesium alloy; Grain refinement; Tensile properties

1. Introduction

Magnesium is an attractive engineering material for the transportation industry because of its high specific strength, good damping capacity, excellent castability, and superior machinability. The relatively poor high-temperature strength of commercial magnesium alloys, however, limits their applications to components working at relatively low temperatures. The most widely used commercial magnesium alloys, such as AM60B and AZ91, for example, can only be used at temperatures up to 120 °C, due to the relatively low thermal stability of $Mg_{17}Al_{12}$ [1], the main strengthening phase in the Mg–Al alloy systems.

Developing magnesium composites by reinforcing the matrix with phases that are thermally stable has been widely explored for improving the high-temperature mechanical properties. Both ceramics (such as SiC [2] and Al_2O_3 [3]) and elemental metals (such as Ni [4] and Cu [5]) have been externally added into magnesium matrix in a fibrous or particulate form as reinforcements. The ceramic reinforcements share a number of common characteristics, including high hardness, high strength, and good thermal stability, thus significantly enhancing the material strengths at both room and high temperatures. However, ceramic materials normally have poor wettability with molten magnesium alloys and low thermal compatibility with the metal matrix. On the other hand, elemental metals such as Ni and Cu have a much greater density than that of magnesium. Use of such reinforcements not only comprises the lightweight of the final composites, but also makes it challenging to uniformly distribute these reinforcing materials in the melt. Intermetallic compounds with high thermal stability, such as nickel aluminide, are considered promising reinforcements for magnesium alloys. For instance, Al_3Ni has an elastic modulus of between 116 and 140 GPa [6,7], density of 4.00 g/cm^3 [8], and melting point of 854 °C [6], and can be an effective reinforcement for magnesium alloys. In this study, the in situ formation behavior of nickel aluminide intermetallic compounds in AM60B alloy is investigated, and the effects of the intermetallic compounds on tensile properties are examined.

2. Experimental methods

2.1. Sample preparation

The composition of AM60B magnesium alloy is given in Table 1. Melting was performed in a vacuum induction furnace using a plain carbon steel crucible, as schematically shown in Fig. 1. The furnace was first pumped down to a vacuum of 10^{-4} Torr before backfilled with Ar to approximately 100 Torr. Ni was added into AM60B melt in the forms of powder or wire.

* Corresponding author. Tel.: +1 519 430 7042; fax: +1 519 430 7064.
E-mail address: xingyang.liu@nrc.gc.ca (X.Y. Liu).

0921-5093/$ – see front matter.
doi:10.1016/j.msea.2006.03.062

Table 1
The nominal composition (specification) of AM60B alloy

Element	Content (wt.%)
Al	5.6–6.4
Mn	0.26–0.5
Zn	<0.2
Si	<0.05
Cu	<0.008
Fe	<0.004
Ni	<0.001
Mg	Balance

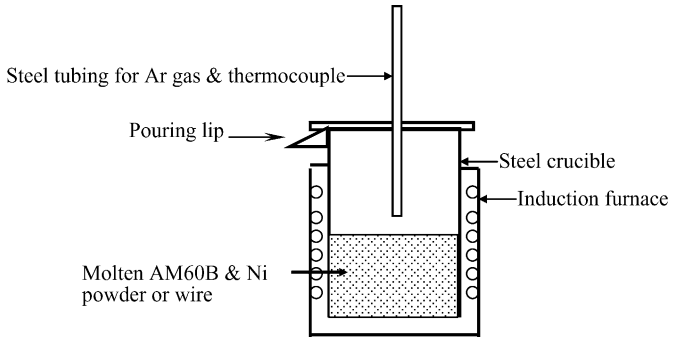

Fig. 1. Schematic illustration of the melting setup.

The powder used has a purity of 99.8% and an average particle size of 10–15 μm. The concentration of Ni powder in the alloys was aimed at 0.5 and 5 wt.%, respectively. The Ni powders were placed between two AM60B blocks in the crucible. After the AM60B block was melted, a carbon steel tubing for argon gas and thermocouple was lowered into the molten alloy, and argon gas was bubbled through the melt. The Ni wire used had a diameter of 1 mm. It was tied to the steel tubing and was lowered into the melt after the magnesium block became molten. The concentration of nickel in the alloy introduced in the wire form was 0.5 wt.%. The effect of argon gas agitation was studied by making two identical melting runs with and without argon gas bubbling. In all cases, the melting temperature was 700 °C and the melting time was 30 or 60 min. Following the melting, the molten alloy was tilt-poured into a steel receiving crucible kept at room temperature. After pouring, it was observed that a solid piece remained at the bottom of the melting crucible for the alloys with Ni powder addition. The size of the remaining solid piece was larger for longer melting time and for the alloy with a higher concentration of Ni addition. For comparing the effect of nickel addition, an AM60B alloy without nickel was cast into a receiving crucible after melting for 2 and 60 min, respectively, at 700 °C without bubbling of argon gas. The experiments of different melting parameters and the corresponding samples are summarized in Table 2.

2.2. Material characterization and tensile tests

For microstructure characterization and composition analysis, samples were cut from the cast ingots and analyzed using an Olympus PMG3 optical microscope as well as a Hitachi S-3500 scanning electron microscope (SEM) with an energy dispersive spectrometer (EDS). Furthermore, particles in the alloy were extracted from the ingot in an ethanol solution containing 25 vol.% acetic acid, and subsequently analyzed using SEM/EDS and a Philips Xpert X-ray diffractometer to examine the phase constitution.

Flat specimens cut from the cast ingots were used for tensile tests. The specimens had a total length of 100 mm and a gauge length of 25 mm. The width and thickness of the gauge length section were 6 and 3 mm, respectively. Tensile tests were carried out using an INSTRON 8516 machine at a crosshead speed of 10 mm/min. Five specimens were tested for each melted sample.

3. Experimental results

3.1. Microstructure and phase compositions

The microstructures of the samples solidified at the bottom of the melting crucible (4-RE and 5-RE) are shown in Fig. 2. The sample with 5 wt.% of Ni powder addition (5-RE) illustrates a high density of coarse particles with polygonal cross-sections and up to 10 μm in size (Fig. 2a). The sample with 0.5 wt.% of Ni powder addition (4-RE) shows lamellar shaped precipitates (labeled with B and C in Fig. 2b) accompanied by a small amount of eutectic microstructure (labeled as A in Fig. 2b). The average compositions of these phases analyzed by EDS were shown in Table 3. It is clear that the particles in both samples are nickel rich, and were most likely due to the sedimentation of the heavy particles to the bottom of the crucible during melting. In contrast, no such solidified residues were observed in the melting crucible

Table 2
Different treatments of the samples

Treatment	Sample designation
1. Melted for 2 min without Ni addition and without bubbling of argon	1-IN: ingot cast into the receiving crucible
2. Melted for 60 min without Ni addition and without bubbling of argon	2-IN: ingot cast into the receiving crucible
3. Melted for 60 min with 0.5 wt.% Ni powders added and with bubbling of argon	3-IN: ingot cast into the receiving crucible 3-RE: remainder in the melting crucible
4. Melted for 30 min with 0.5 wt.% Ni powders added and with bubbling of argon	4-IN: ingot cast into the receiving crucible 4-RE: remainder in the melting crucible
5. Melted for 30 min with 5.0 wt.% Ni powders added and with bubbling of argon	5-IN: ingot cast into the receiving crucible 5-RE: remainder in the melting crucible
6. Melted for 60 min with 0.5 wt.% Ni wire added and without bubbling of argon	6-IN: ingot cast into the receiving crucible
7. Melted for 60 min with 0.5 wt.% Ni wire added and with bubbling of argon	7-IN: ingot cast into the receiving crucible

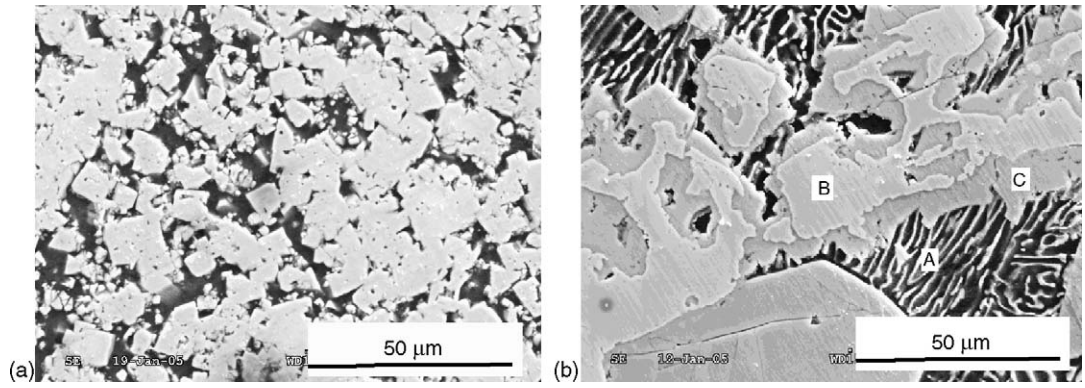

Fig. 2. SEM microstructures of the solid piece remaining in the melting crucible: (a) sample 5-RE (5 wt.% Ni); (b) sample 4-RE (0.5 wt.% Ni).

Table 3
Compositions (wt.%) of the phases shown in Fig. 2 by EDS analysis

	Element				
	Mg	Al	Mn	Fe	Ni
Particles in 5-RE (Fig. 2a)	0.5	24.7	1.9	Undetected	72.9
Eutectic phase (A) in Fig. 2b	64.4	0.7	Undetected	Undetected	34.9
Particle B in Fig. 2b	0.2	20.0	0.9	0.1	78.8
Particle C in Fig. 2b	26.5	4.2	0.6	0.5	68.2

when the 0.5 wt.% of nickel was added to the melt in the wire form, clearly indicating the processing advantage of using wire instead of powder.

The SEM micrograph of the extracted particles from samples with 0.5 wt.% powder addition (4-RE) is illustrated in Fig. 3. The cube-like shape and relatively large size of the particles indicated that these particles were formed in the liquid phase. EDS analysis revealed that the composition of the particles were 70.2 wt.% Ni–22.4 wt.% Al–2.3 wt.% Mn–0.4 wt.% Mg–4.7 wt.% O. X-ray diffraction pattern of the extracted particles is illustrated in Fig. 4. The main phases in the extracted particles were $Al_{0.42}Ni_{0.58}$ aluminide [9] and $Al_{60}Mn_{11}Ni_4$ [10]. No peaks for elemental Ni were found, indicating that all the nickel was in the intermetallic form. Similar microstructure was found in samples with different amounts of Ni powder addition (3-RE, 4-RE and 5-RE), except that the solidified mass at the bottom of the melting crucible was much greater in the sample with 5 wt.% Ni powder addition (5-RE), indicating that increase in Ni content promoted the formation of the coarse $Al_{0.42}Ni_{0.58}$ aluminide.

The effect of melting time, gas agitation and Ni addition on microstructure is shown in Fig. 5. Longer melting time (60 min) along with argon gas agitation resulted in a higher density of particles than the sample with shorter melting time (2 min) without argon gas agitation.

The optical micrographs of samples 1-IN (no Ni addition, no Ar bubbling), 2-IN (no Ni addition, with Ar bubbling), 6-IN (0.5 wt.% of Ni wire, no Ar bubbling) and 7-IN (0.5 wt.% of Ni wire, with Ar bubbling) are shown in Fig. 6. The average grain size of ingot 1-IN, 2-IN, 6-IN, and 7-IN was around 400, 200, 200, and 150 μm, respectively, corresponding to an increase in the density of the particles formed in the samples. The results showed that both longer melting time and bubbling of argon gas was beneficial to the in situ formation of the particles and grain refinement. Fig. 6 also shows that most of the particles were located within the grains.

The compositions of the matrix and particles in samples 1-IN, 2-IN, 6-IN and 7-IN obtained by EDS analyses were shown in Table 4. The matrix compositions of the four samples were essentially the same, close to the nominal composition of

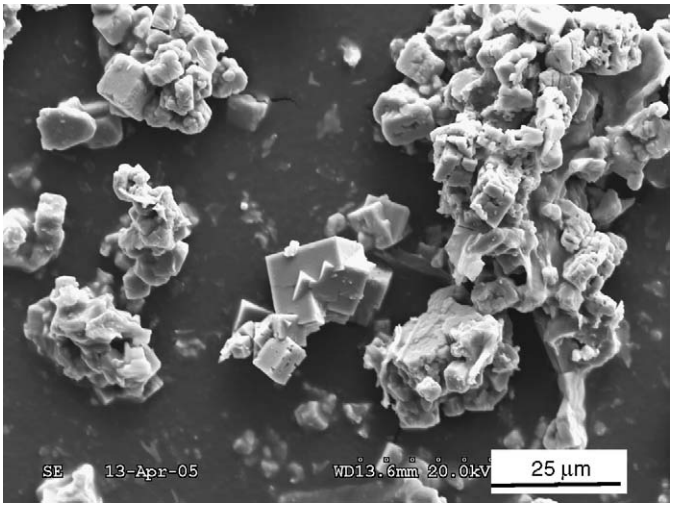

Fig. 3. The SEM image of the particles extracted from sample 4-RE.

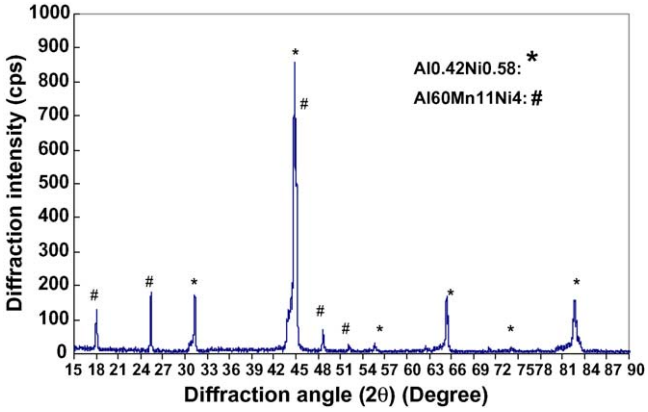

Fig. 4. The (Cu Kα) XRD pattern of the extracted particles from sample 4-RE.

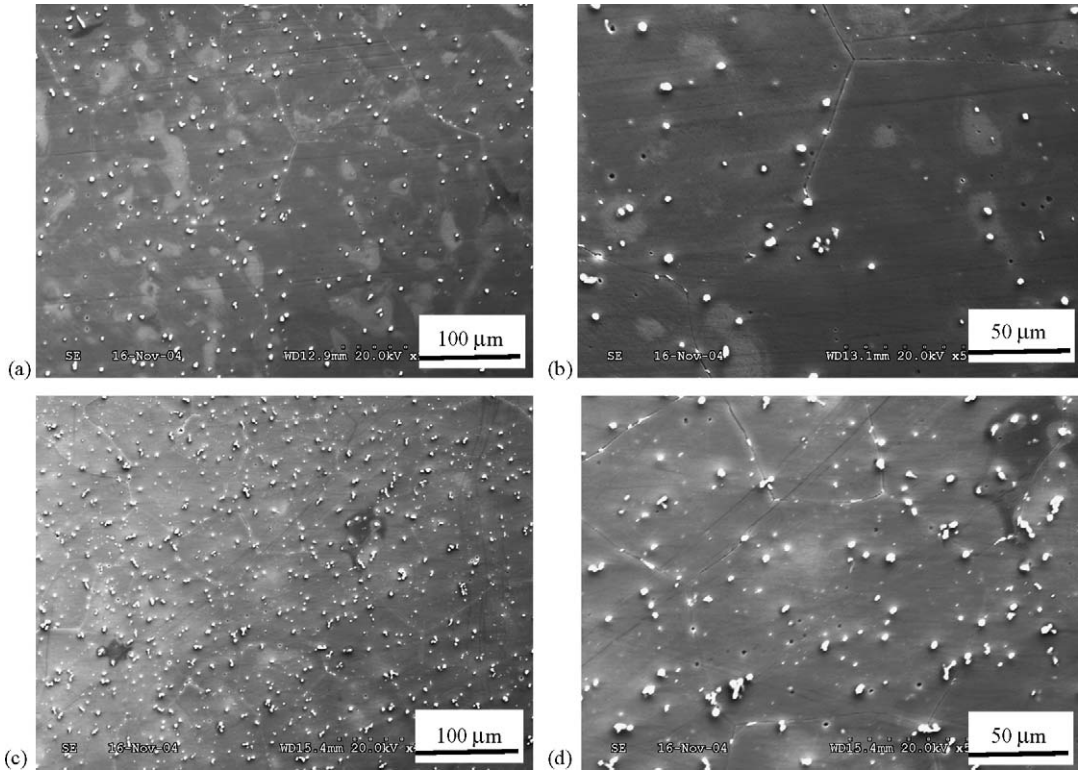

Fig. 5. SEM micrographs of cast samples: (a) and (b) 1-IN; (c) and (d) 7-IN.

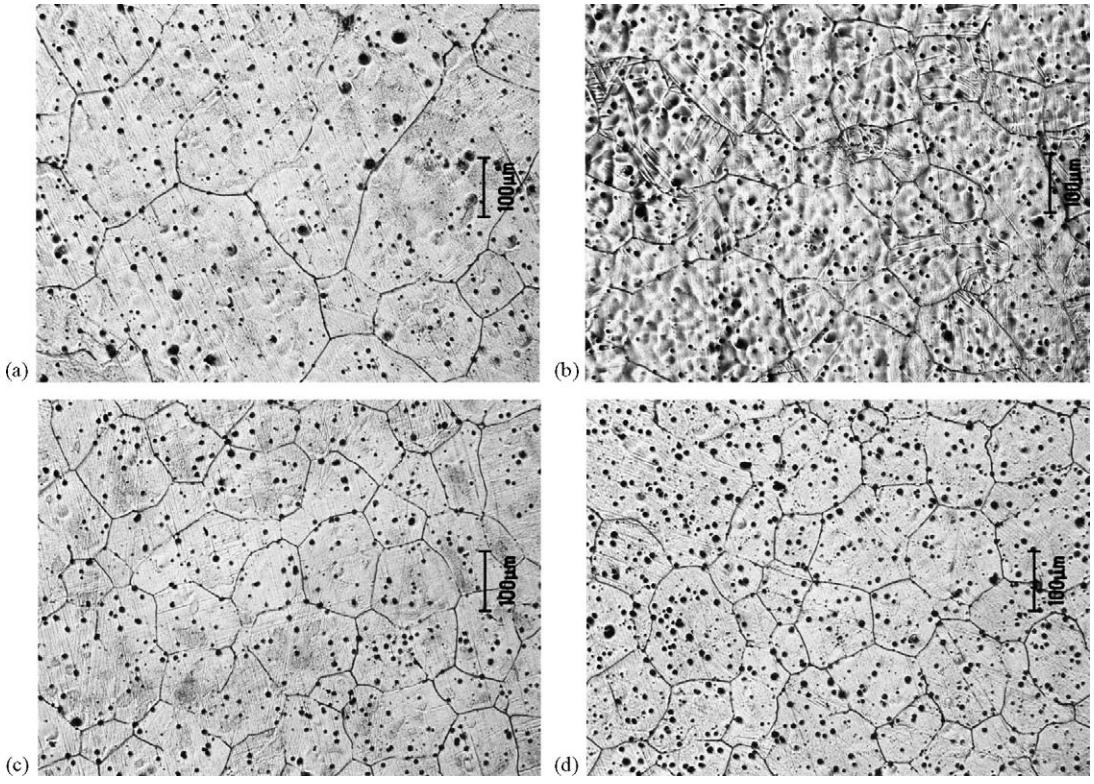

Fig. 6. The optical images of the cast ingot: (a) sample 1-IN; (b) sample 2-IN; (c) sample 6-IN; (d) sample 7-IN.

Table 4
Matrix and particle compositions in cast ingots (wt.%) by EDS analysis

	Element					
	Al	Mn	Ni	Fe	O	Mg
Sample 1-IN						
Matrix	4.9	Undetected	Undetected	Undetected	2.0	Balance
Particle	36.7	48.0	Undetected	Undetected	3.7	Balance
Sample 2-IN						
Matrix	4.2	Undetected	Undetected	Undetected	2.8	Balance
Particle	21.6	20.8	Undetected	Undetected	14.6	Balance
Sample 6-IN						
Matrix	4.8	Undetected	Undetected	Undetected	2.6	Balance
Particle	22.2	16.5	9.9	0.5	7.8	Balance
Sample 7-IN						
Matrix	4.6	Undetected	Undetected	Undetected	2.1	Balance
Particle	21.7	14.6	10.5	0.7	9.9	Balance

AM60B. However, the compositions of the particles in these four samples were quite different. The particles in sample 1-IN and 2-IN contained mainly Mg, Al, Mn, and oxygen, while the particles in samples 6-IN and 7-IN contained a significant amount of Ni along with a minor amount of Fe, in addition to Mg, Al, Mn, and oxygen. It is unclear where the oxygen comes from. Since the melting was conducted under an argon atmosphere in a closed vacuum chamber, it was unlikely that the oxygen was picked up during melting. Considering that the samples were finish polished with 0.05 μm alumina abrasive particles, it is suspected that the oxygen present in the EDS data might be the result of surface contamination caused by embedding of fine alumina abrasive particles into the soft Mg matrix during sample preparation.

SEM/EDS analysis showed that the extracted residues from samples 1-IN and 2-IN had similar compositions and shapes. SEM image of the particles extracted from sample 2-IN are shown in Fig. 7. There were two types of particles present in the extracted residues. One was dark and large, with a size ranging from 20 to 50 μm. The other was bright and small, with

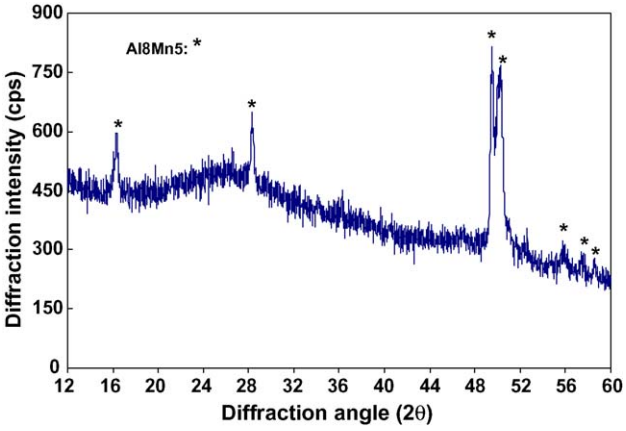

Fig. 8. The (Co Kα) XRD pattern for the particles extracted from 2-IN ingot.

a size around 2 μm. The SEM images also illustrate that the fine and bright particles were attached to the surface of the dark and coarse particles. EDS analysis revealed that the dark and coarse particles had a composition of 41.6 wt.% Al–58.1 wt.% O–0.30 wt.% Mg, and the bright and fine particles had a composition of 34.3 wt.% Al–59.7 wt.% Mn–5.7 wt.% O–0.3 wt.% Mg. The EDS analysis of the two types of particles indicated that the dark and coarse particle was aluminum oxide while the bright and fine particle was a manganese aluminide. The XRD diffraction analysis of the extracted particles from sample 2-IN showed that the main constituent of the extracted residues is Al_8Mn_5 [11], as shown in Fig. 8. Aluminum oxide, however, was not detected by XRD from the residues. The most likely reason for the absence of the aluminum oxide peaks in the XRD spectrum is that the aluminum oxide is in amorphous form. Because no aluminum oxide particles were observed by SEM/EDS analysis of the bulk 1-IN and 2-IN ingots, it is believed that the coarse aluminum oxide particles were formed during the extraction process.

The extraction residue from sample 7-IN consisted of particles with a size around 5 μm, as shown in Fig. 9. These fine particles had a composition of 48.3 wt.% Al–23.9 wt.%

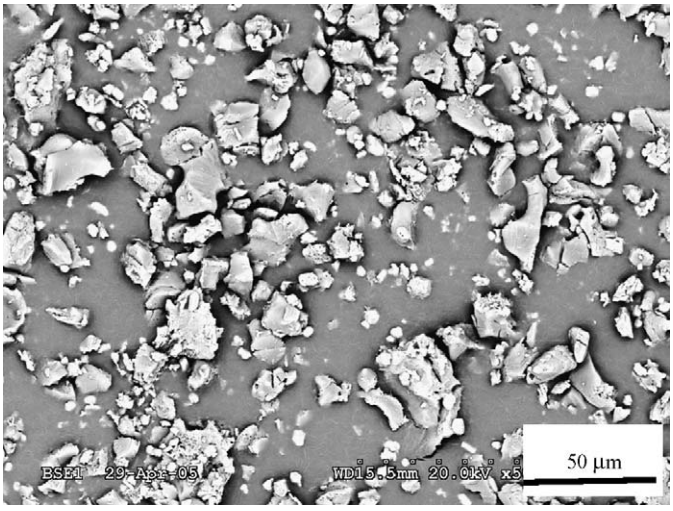

Fig. 7. SEM images of the extracted particles from sample 2-IN.

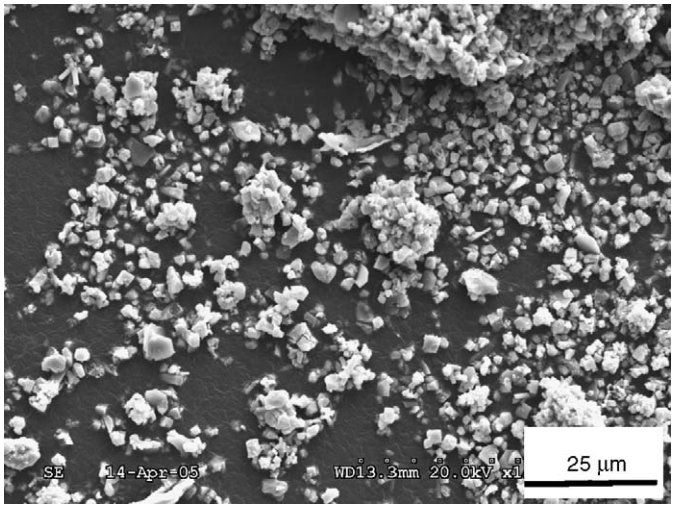

Fig. 9. SEM image of particles extracted from sample 7-IN.

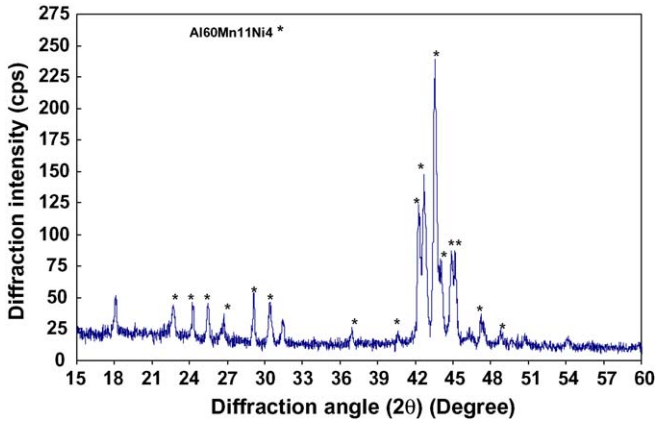

Fig. 10. The (Cu Kα) XRD pattern of the particles extracted from sample 7-IN.

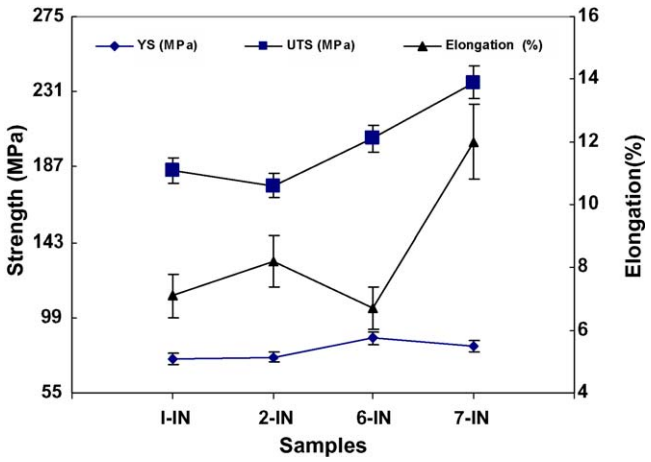

Fig. 11. The tensile performance of the differently processed ingots.

Mn–20.9 wt.% Ni–0.9 wt.% Fe–1.1 wt.% Mg–4.9 wt.% O. XRD pattern of the extracted particles is shown in Fig. 10. The main phase in the extracted residue was revealed to be intermetallic compound $Al_{60}Mn_{11}Ni_4$ [10]. These results confirmed that by adding nickel into the magnesium alloy during melting and properly controlling melting procedures, finely dispersed aluminide particles can be formed in the magnesium matrix.

3.2. Tensile properties

The tensile properties of the materials are shown in Fig. 11. In general, increasing melting time and bubbling argon gas with Ni addition during the melting process augmented the strength and ductility of the material. The ultimate tensile strength increased from around 180 MPa for the samples without Ni addition (1-IN, 2-IN), to 236 MPa for the sample with Ni addition (7-IN). This was accompanied by significant improvement in elongation, increasing from 7% for samples without Ni addition to 12% for the sample melted with Ni and bubbling of argon gas.

The fracture surface morphologies for samples 1-IN and 7-IN are shown in Fig. 12. Both samples displayed similar ductile fracture features, indicating the same fracture mechanism for these two samples.

4. Discussions

Nickel is normally considered a harmful impurity in commercial magnesium alloys, and is avoided to prevent its negative effect on corrosion resistance [12]. In the current study, nickel is intentionally added to investigate its effects on intermetallic formation behavior and on mechanical properties. The experimental results revealed that in the AM60B alloy, nickel exists primarily as the intermetallic compound $Al_{60}Mn_{11}Ni_4$ in the matrix when the concentration of Ni is low and nickel is completely dissolved into the melt, as in the case of sample with 0.5 wt.% of nickel through dissolving fine nickel wires. When Ni was added in the powder form, a high concentration of intermetallic compound $Al_{0.42}Ni_{0.58}$ was found to co-exist with $Al_{60}Mn_{11}Ni_4$ at the bottom of the melting crucible, most likely caused by sedimentation of the nickel powder during melting. The hypothesis was supported by the fact that when Ni was added to the melt through suspended nickel wire, no $Al_{0.42}Ni_{0.58}$ aluminide particles were observed even after extended period of melting. This is because in this case nickel entered the melt in the atomic form through the dissolution of the nickel wires, and therefore minimizes sedimentation. The sedimentation of nickel powders to the bottom demonstrates the challenges commonly encountered in melting materials with ingredients having

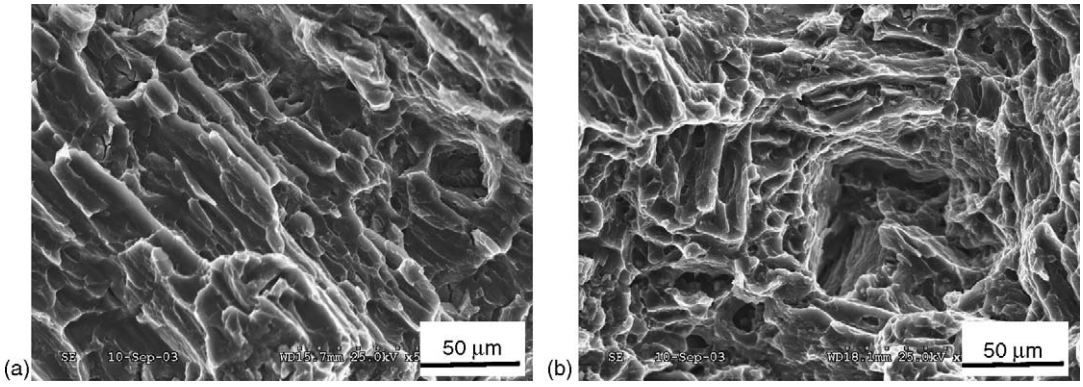

Fig. 12. Fracture surface morphology of samples 1-IN (a) and 7-IN (b).

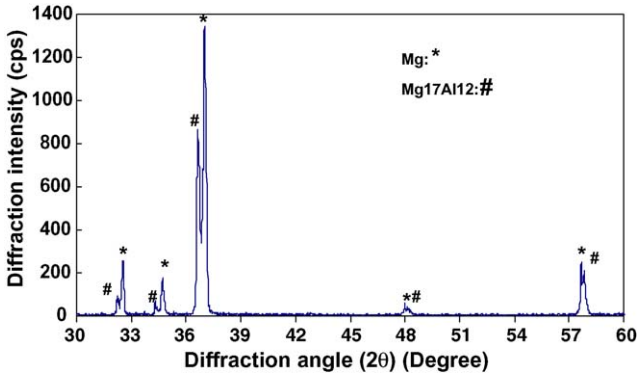

Fig. 13. The (Cu Kα) XRD pattern of ingot 1-IN.

significantly different densities. The segregation also made it very difficult to accurately control and assess the nickel concentration in the bulk of the cast ingots. Clearly, the control of nickel distribution in the melt is critical for homogeneous distribution of the intermetallic compounds formed.

The formation behavior of manganese–nickel aluminide particles in the alloy depends on processing parameters, such as melting time and gas agitation. This can be understood because dissolution of Ni into the molten alloy is an essential step for the formation of Al–Mn–Ni compounds. Long melting time and gas agitation both promote the dissolution of nickel into the melt and, hence, facilitate the formation of manganese–nickel aluminide particles. In addition, gas agitation also promotes the chemical reactions between Al, Mn, and Ni.

The formation of manganese–nickel aluminide particles in the melt will result in the consumption of aluminum and lead to reduced quantity of the $Mg_{17}Al_{12}$ precipitation in the material, which is supported by XRD diffraction analysis of the bulk samples, as shown in Figs. 13 and 14. Clearly, the intensity of the $Mg_{17}Al_{12}$ peaks decreased when $Al_{60}Mn_{11}Ni_4$ was formed as a result of nickel addition.

Both the strength and ductility of the AM60B alloy with nickel addition increased with longer melting time and argon gas agitation. Since grain refinement is the only known strengthening mechanism that increases the strength and ductility of a material simultaneously, it can be expected that grain refinement played a key role in the observed improvement in both strength and ductility, as shown in Fig. 6. However, the fact that the strength and ductility were not steadily improved with the refinement of the grains in ingots 1-IN, 2-IN, 6-IN, and 7-IN, as shown in Fig. 11, also suggests that the change of mechanical properties cannot be solely explained by grain refinement. The increased population density of Al–Mn–Ni particles in the samples with longer melting time and argon gas agitation is expected to also contribute to the strengthening of the material through dispersion strengthening. However, the formation of $Al_{60}Mn_{11}Ni_4$ particles in AM60B alloy is at the cost of reduced $Mg_{17}Al_{12}$ precipitation. The net result of the increased $Al_{60}Mn_{11}Ni_4$ formation and reduced $Mg_{17}Al_{12}$ precipitation seems to increase the strength of the material. The formation of $Al_{60}Mn_{11}Ni_4$ may be particularly beneficial to high temperature strength because $Al_{60}Mn_{11}Ni_4$ is more thermally stable than $Mg_{17}Al_{12}$, judged by their melting temperature.

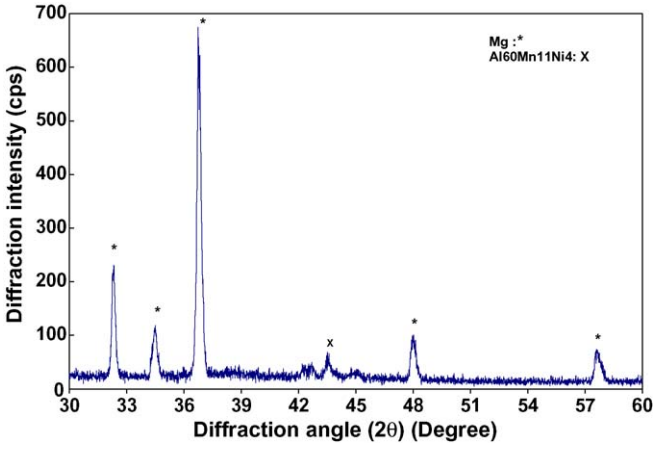

Fig. 14. The (Cu Kα) XRD pattern of ingot 7-IN.

The many desirable characteristics of $Al_{60}Mn_{11}Ni_4$ make it a promising reinforcement phase in magnesium alloys. First, the $Al_{60}Mn_{11}Ni_4$ intermetallic particles maintained a relatively small size and homogeneous distribution in the cast ingot. This is in contrast to some other ceramic particles such as AlN [13] and intermetallic compound such as Mg_2Si [14–19] that are prone to coarsening in the magnesium melt, thus make them ineffective for dispersion strengthening. Secondly, the cost of forming in situ $Al_{60}Mn_{11}Ni_4$ reinforcement is relatively low, as compared to the elements used in other heat resistant magnesium alloys, such as rare earth metals, silver, yttrium and strontium.

5. Conclusions

The in situ formation behavior of the intermetallic compounds in an AM60B alloy with nickel was investigated. The following results were obtained.

- Manganese–nickel aluminide particles ($Al_{60}Mn_{11}Ni_4$) and nickel aluminide ($Al_{0.42}Ni_{0.58}$) particles can be in situ formed in molten AM60B alloy with the addition of nickel.
- The in situ formed manganese–nickel aluminide particles ($Al_{60}Mn_{11}Ni_4$) tend to resist coarsening in the melt and are uniformly distributed in the matrix. In contrast, nickel aluminide ($Al_{0.42}Ni_{0.58}$) particles are prone to coarsening and tend to segregate during the melting process.
- The formation behavior of the intermetallic compounds depends strongly on the Ni content in the AM60B alloy and the way in which Ni is added to the melt. Adding Ni by wire dissolution avoided the sedimentation of Ni to the crucible bottom as encountered in the Ni powder addition, and produced the best mechanical properties.
- The in situ formed manganese–nickel aluminide particles ($Al_{60}Mn_{11}Ni_4$) refine the grains of the matrix and increase the mechanical properties of AM60B.

Acknowledgements

The authors wish to thank Moe Islam for his valuable discussions in the course of this research work. The assistance of Bill Wells, Glen Campbell, and Mike Meinert in conducting the experiments is also gratefully acknowledged.

References

[1] ASM Specialty Handbook, Magnesium and Magnesium Alloys, ASM International, 1999, p. 37.
[2] K. Wu, M. Zheng, C. Yao, T. Sato, H. Tezuka, A. Kamio, D.X. Li, J. Mater. Sci. Lett. 18 (1999) 1301.
[3] V. Sklenicka, M. Svoboda, M. Pahutova, K. Kucharova, T.G. Langdon, Mater. Sci. Eng. A 319–321 (2001) 741.
[4] S.F. Hassan, M. Gupta, J. Alloys Compd. 345 (2002) 246.
[5] S.F. Hassan, K.F. Ho, M. Gupta, Mater. Lett. 58 (2004) 2143.
[6] D.J. Skinner, M. Zedalis, Scripta Metall. 22 (1988) 1783.
[7] Y. Fukui, K. Takashima, C.B. Ponton, J. Mater. Sci. 29 (1994) 2281.
[8] N. Dudzinski, J. Inst. Met. 83 (1954/1955) 444–448.
[9] JCPDS XRD diffraction card 44-1267, 1997.
[10] JCPDS XRD diffraction card 29-0049, 1997.
[11] JCPDS XRD diffraction card 18-0035, 1997.
[12] ASM Specialty Handbook, Magnesium and Magnesium Alloys, ASM International, 1999, p. 28.
[13] H.Z. Ye, X.Y. Liu, B. Luan, J. Mater. Process. Technol. 166 (2005) 79.
[14] E.E. Schmidt, K.V. Oldenburg, Z. Metallkunde 81 (1990) 809.
[15] M. Mabuchi, K. Kubota, K. Higashi, J. Mater. Sci. 31 (1996) 1529.
[16] M. Mabuchi, T. Asahina, K. Kubota, K. Higashi, Inst. Mater. (UK) (1997) 439.
[17] M. Mabuchi, K. Kubota, K. Higashi, Mater. Lett. 19 (1994) 247–250.
[18] M. Mabuchi, K. Kubota, K. Higashi, Miner. Met. Mater. Soc./AIME (USA) (1995) 463.
[19] M. Mabuchi, K. Kubota, K. Higashi, Scripta Metall. Mater. 33 (1995) 331.